Tailoring a coherent control solution landscape by linear transforms of spectral phase basis

Peter van der Walle, Herman Offerhaus, Jennifer Herek, and Aliakbar Jafarpour*

Optical Sciences group, MESA + Institute for Nanotechnology, University of Twente, The Netherlands
**jafarpoura@gmail.com*

Abstract: Finding an optimal phase pattern in a multidimensional solution landscape becomes easier and faster if local optima are suppressed and contour lines are tailored towards closed convex patterns. Using wideband second harmonic generation as a coherent control test case, we show that a linear combination of spectral phase basis functions can result in such improvements and also in separable phase terms, each of which can be found independently. The improved shapes are attributed to a suppressed nonlinear shear, changing the relative orientation of contour lines. The first order approximation of the process shows a simple relation between input and output phase profiles, useful for pulse shaping at ultraviolet wavelengths.

OCIS codes: (320.5540) Pulse shaping; (320.7150) Ultrafast spectroscopy; (350.5030) Phase; (320.5520) Pulse compression.

References and Links

1. P. Brumer, and M. Shapiro, "Control of unimolecular reactions using coherent light," Chem. Phys. Lett. **126**(6), 541–546 (1986).
2. S. Shi, A. Woody, and H. Rabitz, "Optimal control of selective vibrational excitation in harmonic linear chain molecules," J. Chem. Phys. **88**(11), 6870–6883 (1988).
3. J. Werschnik, and E. K. U. Gross, "Quantum optimal control theory," J. Phys. At. Mol. Opt. Phys. **40**(18), R175–R211 (2007).
4. D. Meshulach, and Y. Silberberg, "Coherent Quantum Control of Multiphoton Transitions by Shaped Ultrashort Optical Pulses," Phys. Rev. A **60**(2), 1287–1292 (1999).
5. S. Postma, A. C. W. van Rhijn, J. P. Korterik, P. Gross, J. L. Herek, and H. L. Offerhaus, "Application of spectral phase shaping to high resolution CARS spectroscopy," Opt. Express **16**(11), 7985–7996 (2008).
6. A. C. W. van Rhijn, S. Postma, J. P. Korterik, J. L. Herek, and H. L. Offerhaus, "Chemically selective imaging by spectral phase shaping for broadband CARS around 3000 cm–1," J. Opt. Soc. Am. B **26**(3), 559–563 (2009).
7. R. S. Judson, and H. Rabitz, "Teaching lasers to control molecules," Phys. Rev. Lett. **68**(10), 1500–1503 (1992).
8. B. J. Pearson, J. L. White, T. C. Weinacht, and P. H. Bucksbaum, "Coherent control using adaptive learning algorithms," Phys. Rev. A **63**(6), 063412 (2001).
9. J. L. Herek, W. Wohlleben, R. J. Cogdell, D. Zeidler, and M. Motzkus, "Quantum control of energy flow in light harvesting," Nature **417**(6888), 533–535 (2002).
10. J. Savolainen, R. Fanciulli, N. Dijkhuizen, A. L. Moore, J. Hauer, T. Buckup, M. Motzkus, and J. L. Herek, "Controlling the efficiency of an artificial light-harvesting complex," Proc. Natl. Acad. Sci. U.S.A. **105**(22), 7641–7646 (2008).
11. P. van der Walle, M. T. W. Milder, L. Kuipers, and J. L. Herek, "Quantum control experiment reveals solvation-induced decoherence," Proc. Natl. Acad. Sci. U.S.A. **106**(19), 7714–7717 (2009).
12. P. van der Walle, J. Savolainen, L. Kuipers, and J. L. Herek, "Learning from evolutionary optimization by retracing search paths," Chem. Phys. Lett. **483**(1-3), 164–167 (2009), doi:10.1016/j.cplett.2009.10.049.
13. J. Roslund, and H. Rabitz, "Gradient algorithm applied to laboratory quantum control," Phys. Rev. A **79**(5), 053417 (2009).
14. B. Kohler, V. V. Yakovlev, J. Che, J. L. Krause, M. Messina, K. R. Wilson, N. Schwentner, R. M. Whitnell, and Y. J. Yan, "Quantum control of wave packet evolution with tailored femtosecond pulses," Phys. Rev. Lett. **74**(17), 3360–3363 (1995).
15. C. J. Bardeen, Q. Wang, and C. V. Shank, "Selective excitation of vibrational wave packet motion using chirped pulses," Phys. Rev. Lett. **75**(19), 3410–3413 (1995).
16. Z. Zheng, and A. M. Weiner, "Coherent control of second harmonic generation using spectrally phase coded femtosecond waveforms," Chem. Phys. **267**(1–3), 161–171 (2001).

#118731 - $15.00 USD Received 23 Oct 2009; revised 18 Dec 2009; accepted 18 Dec 2009; published 7 Jan 2010

17. J. Roslund, M. Roth, and H. Rabitz, "Laboratory observation of quantum control level sets," Phys. Rev. A **74**(4), 043414 (2006).
18. A. Jafarpour, J. Savolainen, R. de Jong, J. Middag, D. P. Sprünken, P. van der Walle, D. Yang, and J. L. Herek, "Robust orthogonal parameterization of evolution strategy for adaptive laser pulse shaping," Opt. Express **17**(14), 11986–12000 (2009).
19. A. Paeth, "A fast algorithm for general raster rotation," Graphics Interface **86**, 77–81 (1986).
20. P. S. C. Heuberger, P. M. J. van den Hof, and B. Wahlberg, Modelling and identification with rational orthogonal basis functions (Springer, 2005).
21. A. I. Zayed, Handbook of Function and Generalized Function Transformations (CRC Press, 1996).
22. D. Keusters, H. S. Tan, P. O'Shea, E. Zeek, R. Trebino, and W. S. Warren, "Relative-phase ambiguities in measurements of ultrashort pulses with well-separated multiple frequency components," J. Opt. Soc. Am. B **20**(10), 2226–2237 (2003).
23. D. Zeidler, S. Frey, K.-L. Kompa, and M. Motzkus, "Evolutionary algorithms and their application to optimal control studies," Phys. Rev. A **64**(2), 023420 (2001).
24. R. Fanciulli, L. Willmes, J. Savolainen, P. Walle, T. Bäck, and J. L. Herek, "Evolution strategies for laser pulse compression," Lect. Notes Comput. Sci. **4926**, 219–230 (2008).
25. I. A. Walmsley, and C. Dorrer, "Characterization of ultrashort electromagnetic pulses," Adv. Opt. Photon. **1**(2), 308–437 (2009).
26. V. V. Lozovoy, and M. Dantus, "Systematic control of nonlinear optical processes using optimally shaped femtosecond pulses," ChemPhysChem **6**(10), 1970–2000 (2005).
27. T. Brixner, B. Kiefer, and G. Gerber, "Problem complexity in femtosecond quantum control," Chem. Phys. **267**(1–3), 241–246 (2001).

1. Introduction

Many coherent control experiments rely on tailoring the spectral phase profile of a laser pulse to optimize the yield of a photochemical or photophysical process [1]. Once the dynamics (Hamiltonian) of a controllable system are known, functional analysis can be used to find the optimal spectral phase function [2,3]. Using this analytical approach to determine and to traverse the solution space (landscape) is impractical in many cases of interest. An alternative approach is to traverse the landscape by applying well-known phase profiles to the input laser pulse and scan one or more parameters. In addition to such open-loop scans [4–6], an adaptive scheme is often employed to find the optimal phase profile by relying on the computational intelligence of an evolutionary algorithm [7–12].

An important factor affecting the learning capability of an algorithm in a closed-loop experiment, as well as the results of open-loop scans, is the shape of the solution landscape. An ideal optimization landscape has convex contour lines and no local optima or saddle points. While a coherent control solution landscape can have a simple topology [13 and the references therein], the shapes and the relative orientations of contour lines can be complicated. As will be seen later, the presence of noise and distortions in the spectrum of a laser pulse can result in even more structured landscapes.

The goal of this study is two-fold. First, we want to obtain quantitative data and qualitative insight into the effect of linear transforms of spectral phase basis functions on the shape of a solution landscape. The insight into the how's and the why's of engineering contours in a solution landscape can benefit different numerical and analytical optimization procedures. Second, we want to provide a benchmark to assess phase compensation experiments, and compensate for the residual phase of a so-obtained "nearly transform-limited" pulse by better formulation of the phase function to achieve more conclusive open loop scans in a tailored landscape. The existence of residual phase after an incomplete phase compensation step can hinder the interpretation of further pulse shaping experiments. This is especially important when different electronic and vibrational levels are involved in a transition, and a slightly chirped pulse optimizes the process [14,15].

We can achieve both aforementioned goals by considering the maximization of the total energy of the output of the second harmonic generation (SHG) process as a test case. The total energy is maximized when the spectral phase profile of the input laser pulse is a linear (or constant) function of frequency [16]. Previously, Roslund et al. reported a comprehensive study of the reduced landscape of the SHG process with three degrees of freedom [17] and

#118731 - $15.00 USD Received 23 Oct 2009; revised 18 Dec 2009; accepted 18 Dec 2009; published 7 Jan 2010

also a statistical steepest-ascent technique to probe the local structure of the landscape [13]. We reported the changes of a solution landscape in the context of robust and orthogonal parameterization of an evolutionary algorithm [18]. In this work, we study the properties of 1D, 2D, and 3D landscapes of the SHG process by including up to the sixth order phase term. We then demonstrate and discuss tailoring these landscapes.

We show that a reformulation of the spectral phase function, using linear combinations of the original phase basis functions, can reduce the complexities and distortions of the SHG landscape. Such a modified landscape can even have separable parameters, so that the projection of the optimal point on each axis can be found by scanning only that axis. In other words, the optimal point can be found by a series of independent 1D scans, rather than traversing a twisted curve in a multi-dimensional space. We show the significance of this approach in the case of structured spectral profiles, and also investigate the effect of noise. The results are discussed using two viewpoints: analytic geometry and linear operator theory. The modified landscapes are detailed in Section 4 and discussed in Section 5.

2. Modeling spectral phase

Assuming an analytic and a relatively smooth profile for the spectral phase, it can be expanded in a Taylor series with a few terms around the center frequency. We consider the Taylor series up to the sixth order and discard the zeroth- and first-order terms in our simulations, i.e., $\varphi(\omega) = \Sigma(\varphi_n/n!)(\omega-\omega_0)^n$ for $2 \le n \le 6$. All terms in the Taylor expansion of the spectral phase should have not only the same physical dimension, but also the same unit. As such, φ_n has the unit of $rad^{1-n}sec^{-n}$. To be consistent with the literature, we neglect the radians in the unit of φ_n and assume a multiplier of $1rad^{1-n}$ before it.

Choosing the right range for different phase terms in the study of the landscape is important and nontrivial. A symmetric 2D profile, for instance, will look significantly elongated along one dimension by increasing the range of the other dimension. One method to compare different phase terms is to compare the absolute values of two corresponding terms of the Taylor series expansion of spectral phase. However, different values of ω in the spectral range of the pulse result in different numerical results, and it is not trivial to prefer one value to another. An alternative approach, used in our simulations, is to consider the effect of each term on the SHG process separately. For any given phase term, we first find the values that reduce the energy of the SHG signal by 50%. We will then plot all landscapes within these ranges of the coordinates.

The numerical values of different phase orders only make sense, once the center wavelength is chosen; which in practice depends on the intuition of an experimentalist. If by one choice of the center wavelength, a pulse has only an n-th order phase term, by another choice of the center wavelength, the pulse will have the n-th order and all lower-order phase terms, according to the binomial expansion of $\Phi_2(\omega) = \Phi_1(\omega-\Delta\omega) = \varphi_n(\omega-\Delta\omega)^n/n!$, where $\Delta\omega$ is the difference between two estimations of the center wavelength. Geometrically, the difference between two such phase profiles is simply a shift along the frequency axis. However, a simple shift may be associated with a change of the sign and/or magnitude of the chirp or other phase terms.

3. SHG landscapes

Theoretically, a coherent control problem has an infinite-dimensional solution space. We refer to this space as the *global* solution landscape. By modeling the spectral phase with a specific basis set, such as polynomials, a specific subset of the landscape is created. Unless otherwise stated, the term "solution landscape" refers to such subsets of the global landscape, parameterized with polynomials, in the rest of this article. These landscapes may have similar or different geometrical and topological features, such as local optima, compared to each other and also compared to the global landscape.

#118731 - $15.00 USD Received 23 Oct 2009; revised 18 Dec 2009; accepted 18 Dec 2009; published 7 Jan 2010

By considering the SHG process, the fitness is defined as the energy of the SHG electric field associated with a given phase function, normalized to the energy of the SHG electric field associated with zero phase. The SHG electric field (envelope) is simply an autoconvolution of the fundamental electric field (envelope), under the slowly-varying envelope, very thin crystal, and non-depleted pump approximations [16]. The 1D landscapes of the SHG process for different phase orders are shown in Fig. 1 (left). The amount by which the SHG energy drops as a result of introducing a given spectral phase order has been shown for orders ranging from two to six. We consider a range of each phase term, over which the SHG energy is reduced to half of the SHG energy of a transform-limited pulse. The maximum values of these five phase orders are $\varphi_{2,max} = 453fs^2$, $\varphi_{3,max} = 2.6x10^4fs^3$, $\varphi_{4,max} = 7.85x10^5fs^4$, $\varphi_{5,max} = 6.98x10^7fs^5$, and $\varphi_{6,max} = 4.14x10^9fs^6$. The input laser pulse has a Gaussian spectrum centered at 800nm with a FWHM bandwidth of 35nm.

As the phase order increases, the magnitudes of the slope and curvature at the origin ($\varphi = 0$) increase, while they decrease at the tails of the curves (cross-sections). As a result, the inflection point of each curve approaches the origin as the order increases. As will be seen later, different slopes and curvatures give rise to complicated patterns in higher-order landscapes, especially when two phase terms partially cancel out.

Another important feature of the 1D landscapes is their symmetries. This is not the result of using a symmetric Gaussian spectrum in our simulations. Rather, it is a fundamental property of the SHG process and originates from the fact that $\varphi(\omega)$ and $-\varphi(\omega)$ produce the same SHG energy for any arbitrary phase profile and spectrum. An important practical application of this property is the possibility of verification and compensation for a possible residual phase after an SHG optimization. Assuming that a residual phase dominantly comprises one phase order, it can be compensated by subtracting the peak offset (from zero phase) in the corresponding phase scan profile from the phase of the pulse. The estimation of a residual phase with different phase orders is not trivial, though. Figure 1(right) shows that scanning the cubic phase with a constant background phase of $\varphi_5 = \varphi_{5,max}/4$ results in a peak at an offset value of the cubic phase and an asymmetric trace. A similar scan of the cubic phase with a background phase of $\varphi_2 = \varphi_{2,max}$ results in two maxima at two offset values of the cubic phase, a minimum at $\varphi_3 = 0$, and a symmetric trace. In both cases, the peak values and the curvature magnitudes (at peaks) are smaller than corresponding values in Fig. 1(left) for the φ_3 scan with zero background. A comparison of the profile and the curvature of a measured trace with those of the ideal background-free trace, as in Fig. 1 (left), is insightful but not readily conclusive in the estimation of background phase. This observation leads us to the investigation of higher-dimensional landscapes.

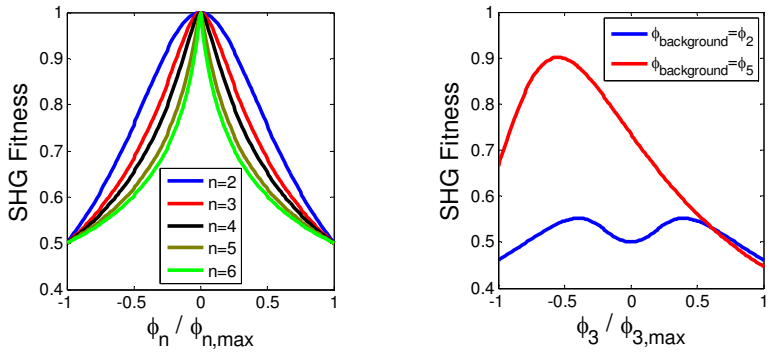

Fig. 1. (left) 1D landscapes of the SHG fitness for different phase orders $\varphi(\omega) = \varphi_n\omega^n/n!$, where ω is the radian frequency of the pulse envelope function and $2 \le n \le 6$, and (right) 1D landscapes of the cubic phase in two cases with the second- and the fifth-order background phase.

#118731 - $15.00 USD Received 23 Oct 2009; revised 18 Dec 2009; accepted 18 Dec 2009; published 7 Jan 2010

The effect of the simultaneous presence of two phase orders *with opposite parities* (even and odd) in the input laser pulse is shown in the 2D plots of Fig. 2. The common point symmetry of all six contours originates from the time-reversal symmetry of the SHG process. Furthermore, the reflection symmetries imply that the SHG energy depends only on the magnitude and the relative signs of different phase terms (with opposite parities).

Comparing different landscapes in Fig. 2 shows that the presence of higher order phase terms results in landscapes with more deviation from a convex pattern. However, in all these cases, it is straightforward to find the projection of the global maximum on each axis, simply by scanning that axis. The projected point corresponds to either the 1D maximum or the midpoint between two 1D maxima. Hence, two 1D open-loop scans can be used in such cases to probe and to compensate for a possible residual phase after a phase compensation experiment.

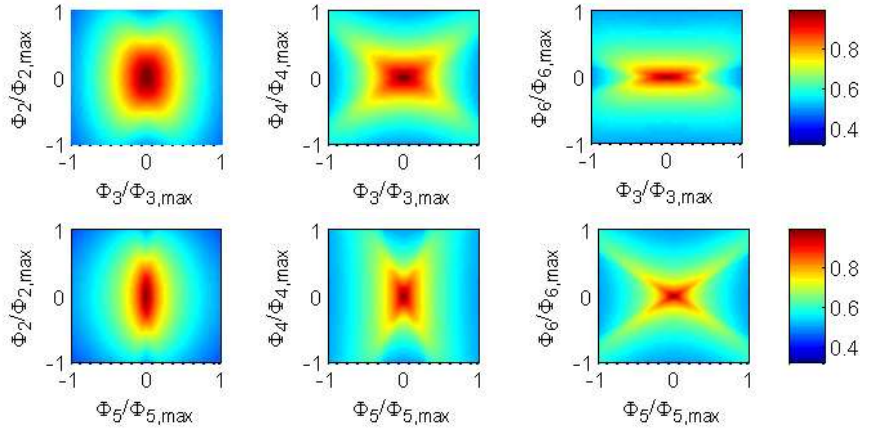

Fig. 2. 2D landscapes of the SHG energy (phase orders with *opposite* parities).

In contrast, the combination of two phase terms *with similar parities* (even or odd), shown in Fig. 3, gives rise to markedly different effects compared to those shown in Fig. 2. While the point-symmetries are still present, the reflection symmetries no longer exist. The contours of constant SHG energy form a twisted pattern for phase orders with similar parities. It will result in a spiral trajectory traversed in a steepest-ascent optimization. This effect is more pronounced as the phase order increases. Also, it is not possible to find the projection of the global maximum (origin) on any axis directly by a 1D scan along that axis.

It is insightful to contrast the plots of Figs. 2 and 3, which use the same color map. In Fig. 3, note the relatively low values of the SHG energy at the corners of the first and the third quadrants and the relatively high values of the SHG energy at the corners of the second and the fourth quadrants, compared to corresponding values in Fig. 2. Two phase terms with similar signs enhance each other, and two phase terms with opposite signs partially cancel each other out in the plots of Fig. 3.

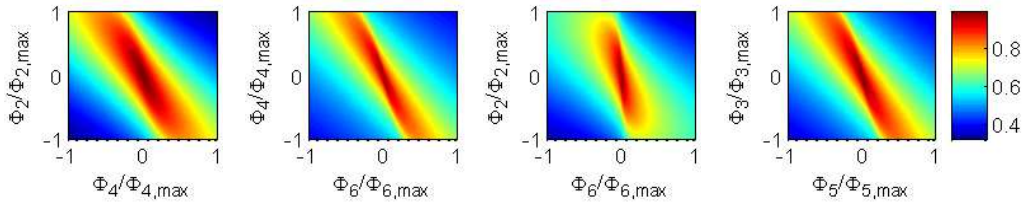

Fig. 3. 2D landscapes of the SHG energy (phase orders with *similar* parities). Contour plots use the same color map as in Fig. 2.

#118731 - $15.00 USD Received 23 Oct 2009; revised 18 Dec 2009; accepted 18 Dec 2009; published 7 Jan 2010

4. Tailoring the SHG landscapes

We assume that the twisted shapes of the landscapes of similar-parity phase terms, shown in Fig. 3, are caused by some correlation between the two corresponding polynomials. We consider a simple correlation, and assume the existence of a linear "projection" of one function along the other. Let ω_n denote the offset radian frequency normalized to the FWHM bandwidth of the pulse, i.e.; $\omega_n = (\omega-\omega_0)/\Delta\omega$. By replacing ω_n^4 with $\omega_n^4-\eta\omega_n^2$, where η is a dimensionless parameter, we show the resulting 2D landscapes of the second order and (modified) fourth order phase terms (φ_2,φ_4) in Fig. 4. All other simulation parameters are the same as those used for Figs. 1-3.

Figure 4 shows that as the parameter η increases from zero to an optimal value of η_0, the contour lines of the 2D landscape undergo significant changes, eventually finding an almost convex pattern without a noticeable relative rotation. A second change of replacing the second-order polynomial from ω_n^2 to $\omega_n^2-\eta'\omega_n^4$ will rotate the contours, among other possible effects. Hence, by using linear combinations of original phase basis with $\eta_0 = 2.22$ and $\eta'_0 = 1.24$ weight factors, it is possible to achieve non-twisted contours with principal axes parallel to the control axes. The new contours have comparable slopes along both new axes in the vicinity of the origin; i.e., for normalized SHG energies of greater than ~82%. Further scaling of the fourth order function as $\eta"(\omega_n^4-\eta\omega_n^2)$ with $\eta" = 0.6$ will reduce the eccentricity of the elliptical contours, giving comparable scales to phase terms in this 2D landscape, and less sensitivity of optimizations to the initial phase. The landscape shown in the rightmost plot of Fig. 4 is more suitable (compared to the leftmost landscape) for the estimation of a residual phase using either open-loop 2D scans or a steepest-ascent-like optimization.

The aforementioned values of η_0 and η'_0 have been chosen by visual inspection of the shapes and orientations of contour lines after a series of simulations. The goal here is to show the effect and get insight into contour evolutions, rather than focusing on a specific figure of merit for landscape modification. Once a specific figure of merit is defined, a min-max or similar optimization techniques can be used to find the values of η and η' that are "optimal" in the sense of the specific optimization criterion. One such figure of merit (to be minimized) is the distance between the landscape function and its quadratic approximation.

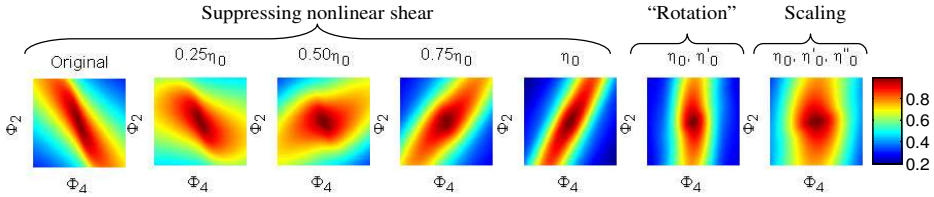

Fig. 4. The evolution of the φ_2-φ_4 SHG landscape by changing the polynomial basis of the phase function $\varphi(\omega) = (\varphi_2/2!)\omega^2 + (\varphi_4/4!)\omega^4 = (\varphi_2/2!)(\Delta\omega)^2\omega_n^2 + (\varphi_4/4!)(\Delta\omega)^4\omega_n^4$, where ω is the radian frequency of the pulse envelope function, $\Delta\omega$ is the FWHM bandwidth, and $\omega_n = \omega/\Delta\omega$. The first five plots on the left show the effect of modification of the fourth order basis function, as it is changed to $\omega_n^4-\eta\omega_n^2$, and the parameter η is varied. The two rightmost plots correspond to an additional change in the second order basis function by modifying it to $\omega_n^2-\eta'\omega_n^4$, and also scaling the fourth order basis function as $\eta"(\omega_n^4-\eta\omega_n^2)$. The general expression for the phase function in all cases is $\varphi(\omega) = (\varphi_2/2!)(\Delta\omega)^2(\omega_n^2-\eta'\omega_n^4) + (\varphi_4/4!)(\Delta\omega)^4\eta"(\omega_n^4-\eta\omega_n^2)$, The numerical values of the modification parameters in the right-most plot are $\eta_0 = 2.22$, $\eta'_0 = 1.24$, and $\eta"_0 = 0.6$. The effect of these transforms on shear is discussed in Section 5.1.

We also consider the impact of such a modification of the phase bases on the other 2D landscapes, as well as on the 3D level sets. Figure 5 shows the modified 2D landscapes corresponding to (φ_2,φ_4), (φ_2,φ_3), and (φ_4,φ_3). Although our modification scheme was merely based one tailoring the φ_2,φ_4 landscape, a fundamental improvement in another 2D landscape (φ_3-φ_4) has made the contour lines convex, without any relative rotation or other artifacts. Regarding the other 2D landscape (φ_2-φ_3), the contour lines have been slightly stretched

#118731 - $15.00 USD Received 23 Oct 2009; revised 18 Dec 2009; accepted 18 Dec 2009; published 7 Jan 2010

along the φ_2 coordinate without relative rotation or other distortions. Note that a line parallel (perpendicular) to the φ_3 axis in the original (modified) φ_2,φ_3 landscape crosses the contours at more than two points, hence a concave contour line.

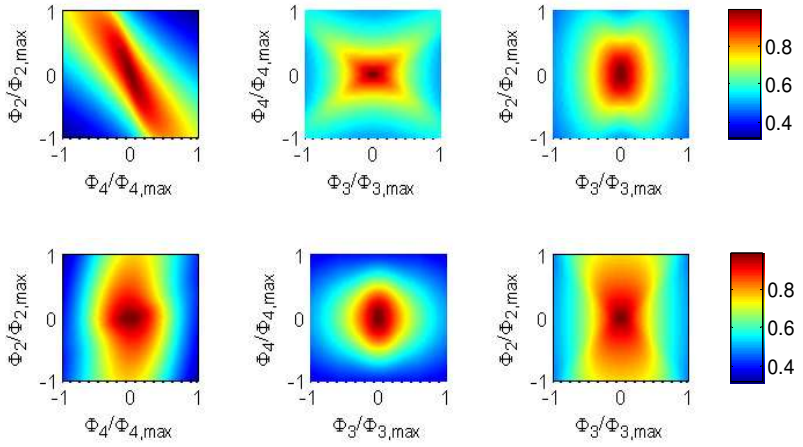

Fig. 5. Original (top) and modified (bottom) 2D landscapes. All contour plots use the same color map.

A 3D level set is the locus of all points in the (φ_i,φ_j,φ_k) space with equal SHG energy. Figure 6 (top row) shows that a level set of the (φ_2,φ_3,φ_4) space is a distorted ellipsoid, whose major axes are not parallel with the φ_i coordinates. As the SHG energy decreases, the torsion of the level sets becomes more visible by the non-uniform distribution of mesh cells and the creation of a white/black region at the bottom/top of a level set. Also, the level sets are elongated along a line with a negative slope in the φ_2-φ_4 plane, since opposite signs of φ_2 and φ_4 partially cancel each other. Furthermore, the orientation of the level sets continuously changes by rotation around the origin in the φ_2-φ_4 plane. A perturbative analysis shows that for nearly transform-limited Gaussian pulses, the 3D level sets are indeed ellipsoids around a global maximum at the origin [17].

In general, a linear transform of the bases of the (φ_2,φ_3,φ_4) space will add six new terms to the original phase bases. Figure 6 (bottom row) shows that using just two terms (associated with η and η') and also scaling by a third term (η'') obtained from the study of the φ_2-φ_4 space, it is possible to reduce the torsion and rotation of the 3D level sets and have their major axes parallel to the coordinate axes in the vicinity of the origin.

#118731 - $15.00 USD Received 23 Oct 2009; revised 18 Dec 2009; accepted 18 Dec 2009; published 7 Jan 2010

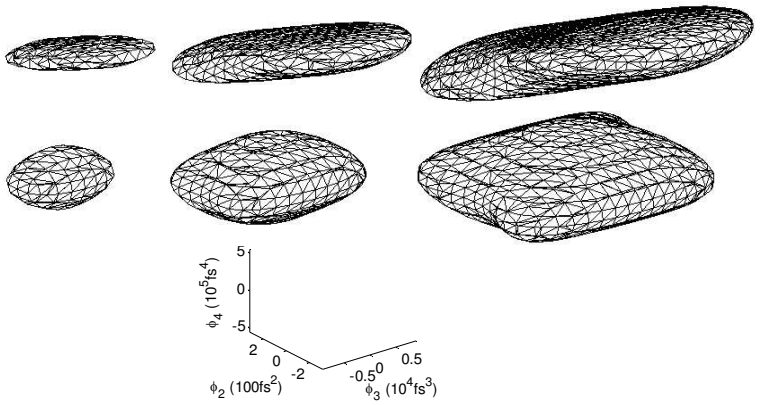

Fig. 6. The level sets of the 3D SHG landscape of the original (top) and modified (bottom) polynomials, corresponding to fitness values of 0.95 (left), 0.90 (middle), and 0.85 (right). All 3D level sets are viewed in the same Cartesian coordinate and from the same angle (azimuth = −37.5°, elevation = 30°). See the attached animated GIF for the evolution of the level sets.

5. Discussion

5.1. Analytic geometry viewpoint

The expansion of the spectral phase function into a basis such as polynomial functions can be written as a matrix product $\varphi(\omega_n) = \Sigma(\varphi_k/k!)\omega_n^k = \Phi\Omega$, where ω_n is the offset and normalized radian frequency, Φ is the row vector of scaled phase terms, and Ω is the column vector of different basis functions.

Replacing $\Phi\Omega$ by $\Phi(A\Omega)$, where A is a non-degenerate square matrix of constant parameters (independent of Φ or Ω), will result in a new basis, with each new basis function being a linear combination of all original basis functions. Alternatively, the modified expression can be written as $(\Phi A)\Omega$. This associative property of matrix multiplication has an important consequence both for numerical and experimental data: Once landscapes are calculated or measured with a given basis, the modified landscapes can be calculated by a matrix transform of the phase parameters, without any new calculation or measurement of the fitness function. For example, the modifications of Section 4 can be seen as a conversion of the original {(1,0),(0,1)} basis vectors to the {(1,-η'),(-ηη",η")} basis vectors in the (φ_2,φ_4) space, without changing the basis functions.

We focus on 2x2 matrices that transform 2D landscapes discussed in Section 4. The result of infinitely countable transforms with such matrices is simply one 2x2 matrix $A = \{a_{ij}\}_{i,j = 1,2}$. Without loss of generality, we assume nonzero diagonal elements to retain the number of independent parameters. By normalizing the matrix to a_{11}, we will end up with three degrees of freedom. This normalization will simply scale the 2D landscape in all directions without any distortion. Once an optimal 3-parameter matrix is found, it can be multiplied by a constant scalar to expand or contract the domain of the fitness function isotropically. Furthermore, by normalizing the second row of the matrix to the diagonal a_{22} element, the landscape will be stretched (or contracted) in one dimension, but otherwise remains undistorted. Aside from two parameters to scale the landscape in horizontal and vertical directions, there are only two (off-diagonal) parameters left to modify the shape of the landscape.

Adding a nonzero off-diagonal element to a 2x2 identity matrix will change it to a shear matrix. A shear transform moves a point (x,y) to (x + my,y) or (x,y + mx), such that the new abscissa (ordinate) is shifted by an amount proportional to the ordinate (abscissa) of the point. The modifications shown in Fig. 4 can be understood as shears in the φ_2-φ_4 plane. Note that a

#118731 - $15.00 USD Received 23 Oct 2009; revised 18 Dec 2009; accepted 18 Dec 2009; published 7 Jan 2010

rotation is equivalent to one scaling and two shears, or just three shears as commonly used in computer graphics [19]. As shown in Fig. 7, in the case of concentric symmetric elliptical contours around the origin, even the result of a single shear looks like that of a rotation. This is why adding a single shear in Fig. 4 (with the coefficient η') can "rotate" the contours of the fitness function.

The second order approximation of a function of two variables in the vicinity of a maximum point is described by a quadratic function. In the case of 2D SHG landscapes, the aforementioned plots and also an analytical approach using the second partial derivative test [17] show that this quadratic function has elliptical contours. Assuming a maximum of 1 and an arbitrary eccentricity of 0.866, we consider the test function $F = 1-(x^2/2^2 + y^2)$, with elliptical contours shown in Fig. 7, to study the effect of shear.

While higher-order approximations of the fitness function can be written in a standard multivariate Taylor series, it is more insightful to consider a function like $F = 1-(x^2/2^2 + [y-f(x)]^2)$, corresponding to a quadric surface with nonlinear shear. This is in agreement with the observation that both 2D and 3D SHG landscapes feature elliptical contours that get distorted, as the fitness decreases. Since contour plots have point symmetry with respect to the origin, the function f(x) must be odd. It includes a linear shear term, a third order nonlinear shear term, and the residual component will be on the order of x^5 or higher: $f(x) = a(LSRx + x^3) + O(x^5)$, where LSR stands for the linear shear ratio, which plays a key role in the shape of the landscape. Assuming $a = -1$ and LSR = + 1, we will achieve rotating contour lines shown in the rightmost plot of Fig. 7, which resemble those in Fig. 3.

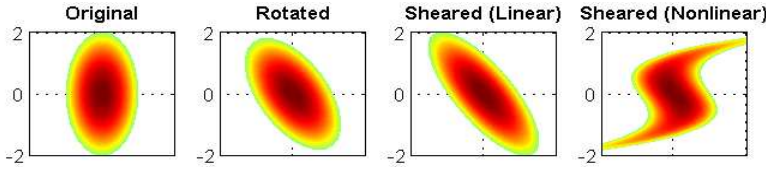

Fig. 7. Contour plots of the elliptic paraboloid $z = 1-(x^2/2^2 + y^2)$ in the original, rotated, and sheared forms.

A more important point about shear is the rotation of contour lines in the case of nonlinear shear and the impact of a linear shear on this distortion. Figure 8 shows the evolution of a quadratic function after a nonlinear shear of one of the coordinate variables. It is seen that the distortion of contour plots is a function of the sign and the value of the LSR, as it is swept from positive to zero and then to negative values.

In the case of LSR = 0 and around the origin, there is the least total shear affecting elliptical contour lines; i.e., negligible rotation or distortion of contours. It can be easily understood by considering the triple root and the flat profile of a cubic function with LSR = 0, as shown in Fig. 8 (rightmost plot). A negative LSR results in a smaller amplitude of the cubic function and hence less nonlinear shear of the (rotated) contours of the elliptic paraboloid over a larger neighborhood of the origin. A positive LSR has the highest nonlinear shear far from the origin, and a larger shear compared to that of the LSR = 0 case, in the vicinity of the origin. So, one should choose the LSR to be zero for the least distortion close to the origin, or a negative value for slightly distorted contours over a larger range.

#118731 - $15.00 USD Received 23 Oct 2009; revised 18 Dec 2009; accepted 18 Dec 2009; published 7 Jan 2010

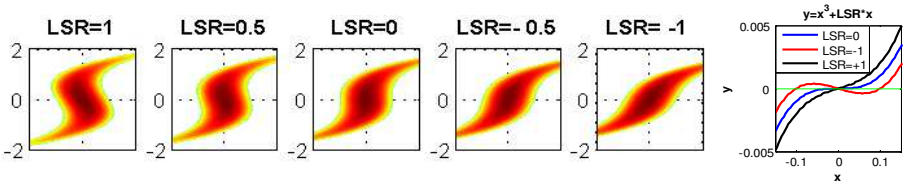

Fig. 8. The five plots of the left panel show the effect of linear shear ratio (LSR) on the contour plots of an elliptic paraboloid distorted with nonlinear shear. The rightmost figure shows the effect of LSR on the range/amplitude of a third order function.

For very large values of LSR, the contour lines will look like a series of parallel lines with a positive or negative slope, depending on the sign of the LSR. Such linear contours imply that the linear shear overshadows not only the nonlinear shear, but also the other parameter. In other words, the two new parameters are no longer independent. So, there is no point in choosing such large values.

In summary, changing the linear shear is not just about rotation. It is also about suppressing nonlinear shear. As shown in Fig. 4, a simple methodology for improving the shape of a 2D landscape is to introduce a linear shear to suppress the nonlinear shear, followed by another linear shear to "rotate" the contours, and finally scaling (if needed). In other words, the elements of the transform matrix *A*, described at the beginning of this Section for changing the phase basis, can be calculated independently and by considering different geometrical features of the landscape.

A more accurate discussion along the same line can also incorporate higher order odd terms of nonlinear shear, and also a shear in both directions of the landscape. However, the similarities of evolving contours in Fig.s 4 (SHG landscape) and 8 (simulated shear) show that even a single cubic shear can explain the distortion and evolution of contour lines.

5.2. Linear operator viewpoint

5.2.1. Linearity and orthogonality

A common approach in analyzing nonlinear systems is "small signal" analysis, in which the first order approximation of the system may result in an acceptable approximation by a (quasi-) linear system. Given the promising results of Section 4 for small phase values, we investigate the possibility of linearizing the SHG process, as $\Delta E_{SHG}(\omega) = L[\varphi(\Omega)]$, where L is a linear operator, $\varphi(\Omega)$ is the spectral phase of the fundamental electric field, and $\Delta E_{SHG}(\omega)$ is the deviation of the SHG field from a transform-limited SHG field.

According to Parseval's identity, the contour line with an energy E_0 in the energy landscape of a non-degenerate linear operator with a countable, complete, and orthonormal basis $\{\psi_n(\Omega)\}$ and an arbitrary output $\varphi(\Omega) = \Sigma c_n \psi_n(\Omega)$ will be the hyper-sphere $\Sigma|c_n|^2 = E_0$. An energy landscape with such contour lines is ideal. The landscape is convex, and all points on a contour line are symmetrically distributed around the origin. Furthermore, the steepest descent trajectory starting from any point is the straight line connecting it to the origin. Finally, all weight factors (c_n) can be found, within a sign factor, independently by 1D scans. Note that the term energy landscape used here refers to the linear operator, and is different from the SHG landscape.

Considering the separability of some phase orders in the SHG landscapes and the possibility of identifying them by individual 1D scans, we pay special attention to the possibility of orthogonal eigenfunctions of a linear operator to describe the SHG process in the small signal regime. If such orthogonal functions exist, there will also be an interesting interpretation of tailoring the SHG landscape done in section 4. By replacing a set of basis functions with their linear combinations, one is indeed performing a numerical Gram-Schmidt orthogonalization [20] by tweaking the weight factors, in the absence of information about a weight function. Note that any two functions with opposite parities are orthogonal for

#118731 - $15.00 USD Received 23 Oct 2009; revised 18 Dec 2009; accepted 18 Dec 2009; published 7 Jan 2010

any arbitrary weight function with even symmetry and over any symmetric subset of the domain of definition of the functions. However, the Gram-Schmidt or similar techniques should be used to orthogonalize similar-parity functions, such as the second- and the fourth-order polynomials.

5.2.2. Small signal approximation and SHG energy

The SHG electric field envelope $E_{SHG}(\omega)$ is an auto-convolution integral of the fundamental electric field envelope $E(\Omega)$ [16]. By separating the amplitude and phase terms of the convolution integral and using Euler's formula to expand the phase term in a McLaurin series, the SHG electric field envelope can be written as the sum of two real series in the form of $E_{SHG}(\omega) = (F_0\text{-}F_2 + F_4\text{-}...) + j(F_1\text{-}F_3 + F_5\text{-}...)$, where $F_n = (1/n!)\int|E(\omega\text{-}\Omega)E(\Omega)|\varphi_t(\omega,\Omega)^n d\Omega$, j is the unit imaginary, and $\varphi_t(\omega,\Omega) = \varphi(\omega\text{-}\Omega) + \varphi(\Omega)$ with $\varphi(\Omega)$ denoting the phase of $E(\Omega)$.

The two series forming the real and the imaginary parts of the SHG electric field envelope comprise the even and odd exponents of the total phase $\varphi_t(\omega,\Omega)$, respectively. The zeroth order term, F_0, is the transform-limited SHG field corresponding to a transform-limited fundamental filed. It follows from the Cauchy Shwarz theorem that the sequence $\{F_{2n}\}$ decreases monotonically, and its contribution to the SHG filed is an alternating series. If the fundamental phase function $\varphi(\Omega)$ is always positive (or negative), the sequence $\{F_{2n+1}\}$ will also monotonically approach zero, and its contribution to the SHG field will be an alternating series, too. For a positive $\varphi(\Omega)$, the contribution of the $\{F_{2n}\}$ and $\{F_{2n+1}\}$ sequences to $E_{SHG}(\omega)$ can be represented by a phasor diagram, as shown in Fig. 9.

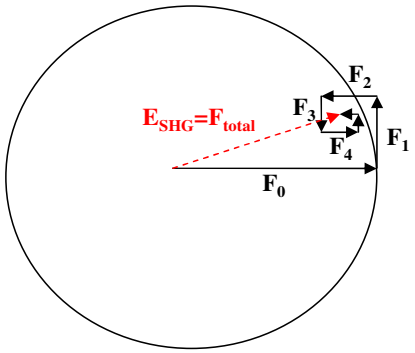

Fig. 9. Phasor diagram showing the contributions of different orders of fundamental spectral phase to the SHG electric field

No matter how small the phase $\varphi(\Omega)$ is, a (quasi-) linear approximation of the SHG process as $\Delta E_{SHG}(\omega) = L[\varphi(\Omega)]$ will always yield a wrong result. Since F_1 adds a quadrature (imaginary) component to F_0, the total SHG field within first order approximation will always have a magnitude greater than that of the transform-limited $E_{SHG}(\omega)$. In order to better understand the contributions of F_1 and F_2 to the SHG energy for small values of phase, we calculate the power spectral density: $P(\omega) = |E_{SHG}(\omega)|^2 \sim F_0^2[1\text{-}2(F_2/F_0) + (F_2/F_0)^2 + (F_1/F_0)^2]$, or simply $P(\omega) \sim F_0^2[1\text{-}2(F_2/F_0) + (F_1/F_0)^2]$, since $(F_2/F_0)^2$ is negligible compared to $2(F_2/F_0)$. This equation has an interesting interpretation. Although F_2 is significantly smaller than F_1 for small values of phase, it contributes linearly and dominantly to the total SHG energy, compared to F_1 with a quadratic contribution to the SHG energy. The second order approximation of the SHG electric field can be valid, and F_2 can have a larger contribution to the magnitude of $E_{SHG}(\omega)$ to make it smaller than that of the transform-limited pulse. For a small constant phase, the contributions of F_1 and F_2 cancel out, as expected.

#118731 - $15.00 USD Received 23 Oct 2009; revised 18 Dec 2009; accepted 18 Dec 2009; published 7 Jan 2010

5.2.3. SHG phase as an integral transform of the fundamental phase

As far as the magnitude of the SHG field and the SHG energy are concerned, the SHG process cannot be linearized, and F_2 dominates F_1. However, the phase of $E_{SHG}(\omega)$ is dominantly determined by F_1, and hence linearly related to the phase of the fundamental field. Note that because of the symmetry of the convolution integral, F_1 can be further simplified as a standard kernel integral: $F_1 = 2\int|E(\omega-\Omega)E(\Omega)|\varphi(\Omega)d\Omega$. The small signal approximation of the phase of the SHG field is $\varphi_{SHG}(\omega)\sim(F_1/F_0)$, which is simply a kernel integral of the fundamental phase normalized to the transform limited $E_{SHG}(\omega)$. The kernel function is merely determined by the spectrum of the fundamental pulse, and is independent of the phase function.

In the case of a Gaussian spectrum $E(\Omega) = \exp(-\Omega^2/2\omega_0^2)$, it can be easily verified that φ_{SHG} is proportional to a scaled Weierstrass transform [21] of the fundamental spectral phase profile: $\varphi_{SHG}(\omega) = 4\pi W[\varphi(y\omega_0/2)]$, where $W[f(y)] = F(x) = (4\pi)^{-0.5}\int f(y)\exp[-(x-y)^2/4]dy$ denotes the Weierstrass transform, and $x = \omega/\omega_0$. As a convolution integral with a Gaussian kernel, Weierstrass transform smoothes a function. It transforms an N-th order Hermite poynomial $H_N(y)$ to x^N, a sinusoidal to a sinusoidal, and an exponential to an exponential.

This simple relation between the fundamental and the SHG phase profiles can be very useful when the SHG signal is used to control a process optimized by a nearly-transform-limited pulse. Direct phase shaping of an SHG signal, especially at ultraviolet wavelengths, faces the challenge of the lower cut-off wavelength of phase masks. However, once the background phase of a pulse is found using SHG optimization, the inverse Weierstrass transform of the required (small signal) SHG phase can be added to the background phase to achieve the desired SHG phase. Such an indirect phase shaping of the SHG signal will increase the useful bandwidth of high-resolution visible pulse shapers by an octave down to ultraviolet wavelengths.

5.3. Robustness

5.3.1. Structured spectrum

We study the effect of the input spectrum on the shape of the solution landscape and the possibility of tailoring the spectral phase bases to modify such a landscape. Figure 10 shows the original (left) and the modified (right) landscapes of the SHG process with the second- and the fourth-order phase terms. The modulated input spectrum is shown in the middle plot in blue. For comparison, the spectrum used in previous simulations is also shown in red. It is seen that a simple modification of the fourth-order basis function, $\omega_n^4-\eta\omega_n^2$ with $\eta = 0.89$, suppresses local maxima close to the origin, and results in a much smoother landscape. A single linear shear reduces (and almost removes) the depth of modulation of the original modulated landscape.

Characterization of a pulse with a structured profile is usually associated with an increased error compared to simpler profiles, because of the finite temporal and spectral resolutions of a measurement setup. Also, conventional self-referenced phase measurement techniques fail to fully measure the phase of a pulse with well-separated spectral components [22]. It can make SHG optimization a more attractive option for such measurements. At the same time, it is important to improve the structured shape of the landscape to achieve an efficient optimization.

#118731 - $15.00 USD Received 23 Oct 2009; revised 18 Dec 2009; accepted 18 Dec 2009; published 7 Jan 2010

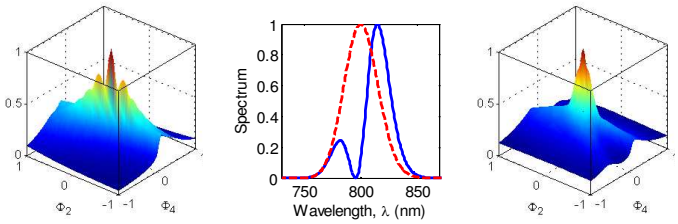

Fig. 10. The original (left) and the modified (right) surfaces of the total SHG energy with the second order and the fourth order polynomial functions. The middle plot shows the original (red) and modulated (blue) input spectra used for the simulations.

5.3.2. Noise

It is known that noise has a negative impact on the learning capability of closed-loop coherent control problems [23,24]. At low levels of signal to noise ratio, the learning process does not start in the first place, as small improvements of the fitness function are comparable or negligible compared to noise level. We studied this effect previously and proposed to use orthogonal functions for robust implementations [18]. Here, we consider a different type of noise, which is more common in coherent control experiments, and study its effect on original and modified φ_2-φ_4 landscapes of the SHG process.

Phase noise is used to model laser beam instabilities, as produced by compressors and stretchers. As different wavelengths of a pulse with angular or spatial chirp propagate along different directions, they can experience slightly different indices of refraction caused by air flow, for instance. Assuming negligible (or constant) Fresnel losses, the total energy of each wavelength after combining different colors can remain essentially constant. However, the perturbation of the delays (and hence phases) of different colors can still be important. Such a laser pulse can have a stable single-shot spectrum, but an unstable single-shot SHG spectrum. The generation of such phase noise in the stretcher part of a chirped pulse amplification (CPA) system will give rise to instabilities of the amplified pulse, detectable by a single-shot measurement of energy. The generation of phase noise in the compressor part of a CPA can affect further phase-sensitive processes, but cannot be detected by a single-shot measurement of energy. Since this noise does not affect the spectrum of the fundamental pulse, it is not expressed in terms of signal to noise ratio. We simply scale this noise and mention the scale factor in each case. If $\varphi(\omega)$ and $\varphi_n(\omega)$ denote the original (noiseless) and modified (noisy) phase functions, we can write $\varphi_n(\omega) = \varphi(\omega) + \varphi_{noise}N(\omega)$, where φ_{noise} is a scale factor with the unit of radians, and the function N is a realization of a random sequence with Gaussian distribution and having zero mean and unity variance. In calculation of each point of the following landscapes, a new realization of the random sequence N is used.

The results of introducing different levels of phase noise to the SHG process are shown in Fig. 11. Both original and modified φ_2-φ_4 landscapes are studied. As the noise level increases, the coherence and the fitness decrease. For a fair comparison, all plots of Fig. 11 have been plotted using the same color map with dark red(blue) representing 1(0). Using different color maps to achieve the best contrast for each plot shows that the main features of the landscape remain essentially the same, even though the heights of the "bumps and dips" increase. Hence, care must be taken in comparing different fitness values associated with two noise levels. The highest fitness values corresponding to all noise levels correspond to the origin (zero phase). However, the fitness value at this point assumes very different numbers in each case. Unless limited by detector sensitivity or algorithm step size/direction, the phase-noise-induced reduced fitness is not associated with an error in estimation of the phase (of the corresponding ideal) laser pulse. This behavior holds in the case of both original and modified landscapes.

#118731 - $15.00 USD Received 23 Oct 2009; revised 18 Dec 2009; accepted 18 Dec 2009; published 7 Jan 2010

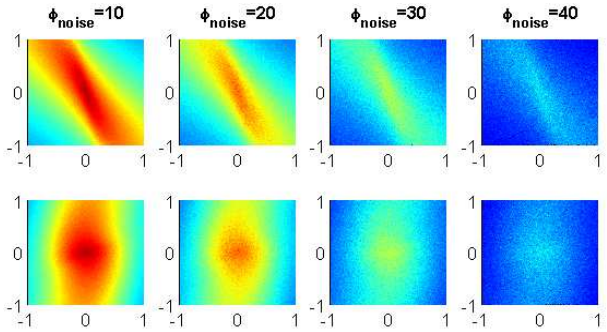

Fig. 11. The impacts of different levels of phase noise on the original (top) and modified (bottom) φ_2-φ_4 landscapes.

Different points in each landscape of Fig. 11 have been calculated with different realizations of the noise signal to consider its stochastic nature. Despite that, it is still important to make sure a landscape pattern is not a function of a specific realization of the noise signal. We repeat the calculation of the fitness landscapes for the case of $\varphi_{noise} = 20$ and modify the color map slightly to achieve the best contrast. Figure 12 shows that all landscapes are *statistically* equivalent and have similar features, even though the fitness values at a specific point may be slightly (determined by noise level) different.

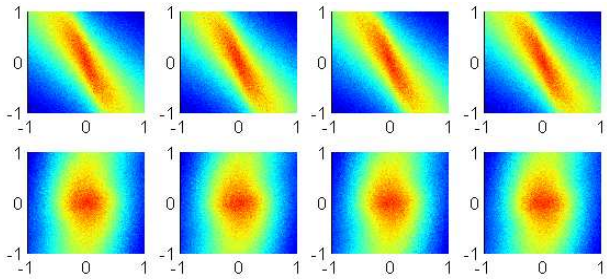

Fig. 12. Four different realizations of the original (top) and modified (bottom) φ_2-φ_4 landscapes for a given level of phase noise.

5.4. Assessment and correction of phase compensation experiments

Conventional self-referenced phase measurement techniques have the advantage of real-time measurement compared to a measurement using an SHG optimization. On the other hand, SHG optimization does not suffer from the direction of time ambiguity [25], geometrical smearing, or sensitivity to the symmetry of the spatial profile for generating two similar replica of a beam. Furthermore, SHG optimization offers more convenience and less numerical errors by using the same coordinate, software, and setup for phase compensation and further pulse shaping.

There are also factors that depend on the implementation of a phase measurement technique, and are not inherent limitations. For example, SHG optimization can be sensitive to local optima. However, tailoring the landscape can remove or suppress local optima, and make the optimization more efficient. A similar argument applies to phase measurement techniques using an optimization for phase retrieval.

An SHG optimization is less sensitive than conventional phase measurement techniques to crystal thickness. If the phase-matching bandwidth is equal to or slightly larger than the bandwidth of the laser pulse, the crystal transfer function will only contribute an amplitude to the integrand of the SHG signal [16]. As such, a transform-limited pulse will still be the optimal solution of an SHG optimization, in the light of Cauchy-Schwarz theorem. However,

#118731 - $15.00 USD Received 23 Oct 2009; revised 18 Dec 2009; accepted 18 Dec 2009; published 7 Jan 2010

the crystal transfer function will completely change the formula of the SHG signal. Given the nonlinearity of the SHG process and intra-pulse interferences generating the SHG signal at different frequencies, a "normalization" of the measured nonlinear signal to the transfer function of the crystal is not trivial. Although this is not an inherent limitation of phase measurement techniques, considering the crystal thickness will result in heavier computation load and is usually avoided.

In general, both conventional phase measurement techniques and SHG optimization can be considered as alternative and complementary techniques, the results of which verify (but not necessarily validate) the results of the other. No matter what technique has been used to estimate and compensate a spectral phase profile, a pulse shaper can be used to probe and compensate residual phase using open-loop scans. Tailored landscapes studied here are crucial for the success of this assessment.

5.5. Alternative parameterizations and processes

Binary basis functions, borrowed from the context of digital communications, form an important and a completely different basis set, used in SHG and other pulse shaping experiments. The fitness maps or "landscapes" associated with these functions have discrete coordinates, representing *symbolic* binary codes of different phase profiles [26]. There can be dramatic differences between the phase profiles (and hence fitness values) of consecutive binary codes, contrary to the landscapes addressed in our study. As such, care must be taken in establishing analogies or developing schemes for the modification of such landscapes.

SHG optimization can be used in spectroscopic applications of pulse shaping, not only to achieve and verify a zero-phase profile, but also to verify the nature of the main optimization. A trivial increase of the fitness function in many spectroscopic experiments originates from an increase of the pulse peak power. Simultaneous application of shaped laser pulses to the main experiment and a test SHG setup, followed by a comparative study of the corresponding fitness functions can differentiate between trivial and nontrivial control mechanisms [27].

6. Conclusions

In conclusion, we have shown that a linear combination of spectral phase basis functions can improve the shape of a coherent control solution landscape, by changing the contour lines towards more convex shapes and suppressing local optima. Such a modification can also result in separable phase terms that can be found independently. The improved shapes of the landscapes are attributed to a suppressed nonlinear shear, changing the relative orientation of contour lines. For the process of second harmonic generation, open-loop scans in such landscapes can be used for efficient verification and compensation of residual phase after an incomplete phase compensation experiment. It is shown that a first-order approximation of the second harmonic generation can correlate fundamental and second harmonic phase profiles via a simple linear transform with an important application in high-resolution pulse shaping at ultraviolet wavelengths.

Acknowledgements

This research has been supported by the Stichting voor Fundamenteel Onderzoek der Materie (FOM, grant number 03TF78-3), which is supported financially by Nederlandse Organisatie voor Wetenschappelijk Onderzoek (NWO).

#118731 - $15.00 USD Received 23 Oct 2009; revised 18 Dec 2009; accepted 18 Dec 2009; published 7 Jan 2010